Vaporization-controlled simplified model for liquid propellant rocket engine combustion chamber design

Vaporization-controlled simplified model for liquid propellant rocket engine combustion chamber design

H Belal[1,3], Ah El-S Makled[2] and M A Al-Sanabawy[1]

[1] Department of Rockets, Military Technical College, Cairo, Egypt
[2] Space Technology Centre, Cairo, Egypt

[3] hbelal@mtc.edu.eg

Abstract. The design of liquid propellant rocket engine (LPRE) is a very complicated process; this is due to two main concerns: First, the requirements to satisfy the issues of performance, stability and compatibility. Second, the complicated, interacting processes inside thrust chamber. In this paper, an attempt to illustrate the importance of different parameters affecting performance, stability and compatibility is performed, followed by extensive study of processes inside thrust chamber. The result of processes study is developing the concept of "rate limiting process" which means that the process that can be considered the most important hence the design can be done mainly by considering it alone. This is done by developing a 1D vaporization-controlled model with its application to two case studies to illustrate model validation and application. It was found that the 1D model is valid as long as the vaporization process is the slowest process in this case the error in computing chamber cylindrical length is ~15%. However, if the mixing process is slow, or the reaction process in gas phase is slow as in the second case study of RFNA/Tonka250 case, the error grow and may reaches 50%

1. Introduction

The design of LPRE thrust chamber needs to consider a large number of different phenomena that occur during the combustion process As a result there are a large number of similarity parameters- e.g. Reynolds, Prandtl, Schmidt numbers in addition to first and third Damköhler numbers- that should be used in designing and scaling of rocket combustors. Hence, scaling of LPRE with complete similarity is found to be practically impossible.

A classical approach to design a liquid propellant rocket engine (LPRE) combustion chamber is Characteristic length approach. This characteristic length is defined as ratio between volume of combustion chamber *starting at injection head till the nozzle critical section) and nozzle critical area. The design procedure moves by selecting the propellant composition then choose a value of characteristic length from the experimental database (table 1). After calculating the required volume, use geometric relation to find dimensions of combustion chamber for different shapes (cylindrical, spherical, ellipsoidal, etc.).

However, this approach does not show how the design parameters e.g. injector design, propellant temperature, etc. affect the performance of the combustion chamber. This makes rocket engineers to turn to the concept of rate limiting phenomena, which defined as the phenomena that control the chemical reaction or heat release process and discarding all other processes for engineering purpose.

Combustion chamber stay-times must be long enough to ensure that all processes are completed before entering the nozzle. The processes occurring in a liquid propellant thrust chamber can be classified into three general categories: atomization/vaporization, propellant mixing, and chemical reaction. Chemical reaction rates are usually not rate-limiting in normal thrust chamber except if combustion is taking place at extreme variation from stoichiometric conditions. The propellant mixing process loss is 0-2% of energy release losses, if the chamber is designed for effective intra-element liquid-phase mixing using criteria similar to the JPL mixing formula [2]. In addition, it was found lengths required to complete gas-phase mixing of propellant is much smaller than required for complete vaporization [3] , this make the vaporization process the rate limiting process and make it the most influential process as some references indicated that 5 % vaporization loss of one of the space shuttle propellants would results in 23 % reduction in polar orbit payload capability[4]. Priem and associates 8at NASA Lewis laboratory performed the definitive work of that period, summarized in Priem and Heidmann [5]. Whereas earlier investigators had utilized limiting case assumptions or unrealistic spray droplet dynamics to achieve closed-form solutions.

Table 1. Values of characteristic length for different propellant combinations [1].

Propellant Combination	L* (m)
Nitric-acid-Hydrocarbon	2-3
Nitric Acid-UDMH	1.5-2
LOX-Ethyl alcohol	2.5-3
LOX-Kerosene	1.5-2.5
Fluorine-Ammonia	1-1.5

In this paper, vaporization-limited one-dimensional model is elaborated then applied to two cases; LOX/Kerosene as an example for cryogenic/storable propellant and RFNA/Tonka250 as an example for earth storable propellant Finally the discussion of results of the two cases are introduced to justify the assumptions of model and declare its limitations.

2. Model

For simplified one-dimensional steady flow in which propellant vaporization is the rate-controlling process, it is assumed that:

- Both reaction and mixing rates in gas phase are infinitely fast; hence the length of chamber is considered the breakup and vaporization lengths only
- No reaction in liquid phase; that means all heat transfer is convective heat transfer from the environment only
- All droplets in the initial spray have the same initial velocity
- Droplets never shatter or coalesce (neglecting secondary atomization)
- Properties of the bulk gas flow correspond to instantaneous stoichiometric combustion

The processes of steady-state mass, momentum, and heat-transfer were divided into small increments during which only small change occurs, a model can be set up for each droplet as shown schematically in figure 1.

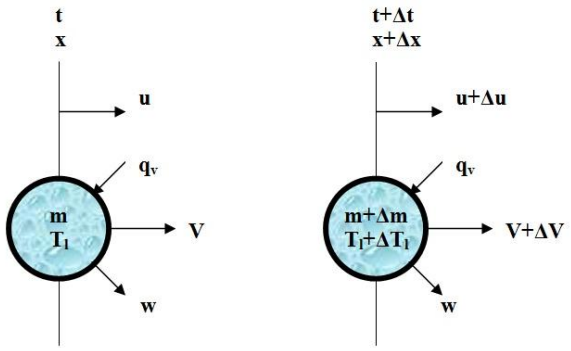

Figure 1. Schematic model of fuel or oxidant droplets vaporizing in rocket engine

3. Governing equations

Mass transfer $$\frac{dm_d}{dt} = w = A_S K \alpha P_{a,s} \quad (1)$$

Heat transfer $$q_v = h A_S \left(T_c - T_l\right) Z \quad (2)$$

Droplet-heating rate $$\frac{dT_d}{dt} = \frac{1}{m c_{p,l}} \left(q_v - w\lambda\right) \quad (3)$$

Droplet acceleration $$\frac{dV_d}{dt} = -\frac{3}{8} C_D \frac{\rho_m}{\rho_l} \frac{U^2}{r_S} \quad (4)$$

Gas velocity $$\frac{u(x)}{u_{fin}} = 1 - \frac{\dot{m}_f(x)}{\dot{m}_{f,in}} \quad (5)$$

Average physical properties

The previous equations require the use of the thermal conductivity, viscosity, and specific heat of the vapor mixture surrounding the droplet. Therefore, the properties were therefore calculated at, the arithmetic average temperature in the film and for a vapor concentration equal to half the concentration existing at the droplet surface.

$$\bar{T} = \frac{T_c + T_l}{2} \qquad k_m = \left(1 - \frac{x_\upsilon}{2}\right) k_a + \frac{x_\upsilon}{2} k_\upsilon$$

$$\mu_m = \left(1 - \frac{x_\upsilon}{2}\right) \mu_a + \frac{x_\upsilon}{2} \mu_\upsilon \qquad \bar{M} = \left(1 - \frac{x_\upsilon}{2}\right) M_a + \frac{x_\upsilon}{2} M_\upsilon \quad (6)$$

$$c_{pm} = \left(1 - \frac{x_\upsilon}{2}\right) \frac{M_a}{\bar{M}} c_{p\,a} + \frac{x_\upsilon}{2} \frac{M_\upsilon}{\bar{M}} c_{p\,\upsilon} \qquad \rho_m = \frac{p\bar{M}}{R T_m}$$

In these relations, subscript *a* refers to the vaporizing material and subscript *b* to the surrounding gaseous material.

Relation between percentages mass vaporized and performance

Incomplete propellant vaporization degrades c* performance in two ways; (1) Incomplete vaporization reduces the total amount of combustion gas produced and (2) If fuel and oxidizer do not vaporize at the same rate, this can make the burned gas mixture ratio different from the injected liquid mixture ratio, thereby affecting the temperature, molecular weight, etc. of the burned gas.

The characteristic velocity c* that can be theoretically realized may be computed from the thermodynamic properties of the combustion products calculated using thermo-chemical calculation programs.

$$\eta_{C^*} = \frac{\left(C^*_{th}\right)_{O_{vap}/F_{vap}}}{\left(C^*_{th}\right)_{O/F}} \frac{\dot{m}_{vaporized}}{\dot{m}_{injected}} = \frac{\left(C^*_{th}\right)_{O_{vap}/F_{vap}}}{\left(C^*_{th}\right)_{O/F}} \%M_{vap} \qquad 7$$

where

A_{cr}	Critical cross section on nozzle
O_{vap}	fraction of oxidant and fuel vaporized
F_{vap}	fraction of oxidant and fuel vaporized
$\left(C^*_{\exp}\right)_{O/F}$	Experimental(measured) characteristic velocity for injected mixture ratio
$\left(C^*_{th}\right)_{O_{vap}/F_{vap}}$	Theoretical characteristic velocity at vaporized mixture ratio
$\left(C^*_{th}\right)_{O/F}$	Theoretical characteristic velocity at injected mixture ratio

4. Model results

4.1. Histories of single droplet of heptane in a cylindrical chamber

In this section, the model is applied to a simple case of single heptane (representative for hydrocarbon) vaporizing in gaseous stream of oxygen (representative of oxygen entering combustion chamber in gas phase) for this case, the input data are given in table 2.

From figure2, it should be note that approximately 25% of total vaporization length was required to attain the wet bulb temperature, with this period of heat up is proportional to square of droplet diameter, and increase with pressure, decrease with increasing ambient temperature. It has been found that the radius curves for high-molecular-weight fuels first increase and then decrease while the curves for low-molecular-weight fuels decrease immediately because the high-molecular-weight fuels initially expand thermally while not losing much mass by vaporization The droplet velocity first decreases because of the drag produced by the low gas velocity, a minimum is reached when the gas velocity equals to droplet velocity. After the minimum point the droplet velocity increase because of the drag produced by the high gas velocity.

Table 2. Data for single n-heptane droplet case

Droplet radius [micron]	75
Initial droplet velocity [m/sec]	30
Chamber pressure [bar]	20
Chamber gas temperature (K)	3100
Initial droplet temperature (K)	280
Chamber contraction ratio	3.15

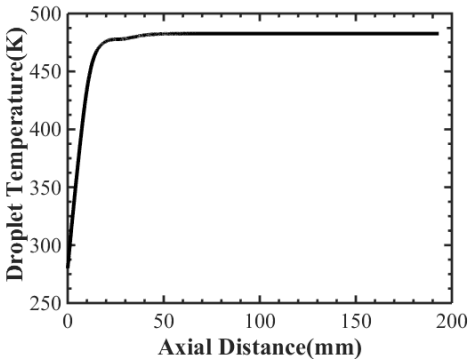

Variation of droplet temperature

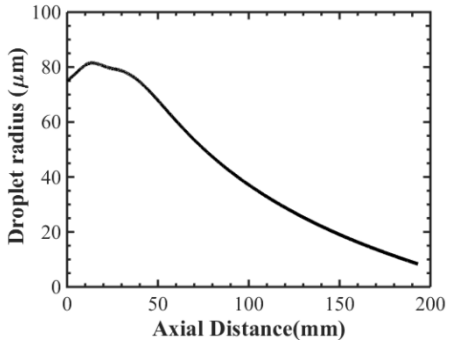

Variation of droplet radius

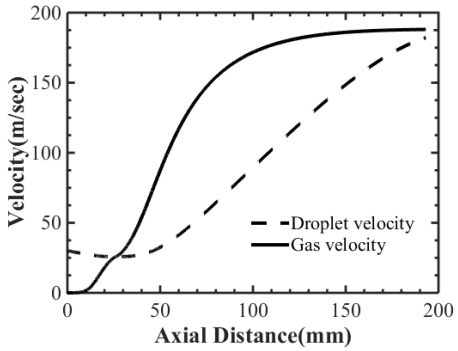

Variation of droplet and gas velocities

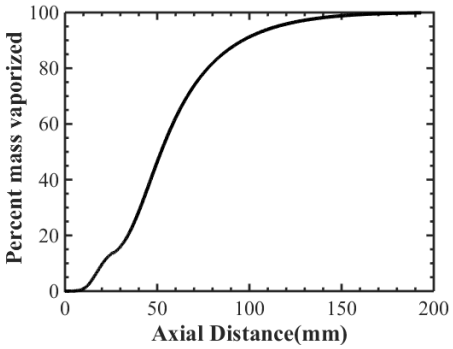

Percentage mass vaporized

Figure 2. Variation of droplet temperature, droplet size, droplet velocity and percentage mass vaporized with axial distance for single heptane droplet

The percent-mass-vaporized curve initially has a very small slope because of the low liquid temperature of the droplet. As the droplet heats up, the slope of the percent-mass-vaporized curve increases. At the end of the droplet lifetime, the slope again decreases because of the decrease in droplet surface area and because the droplet is accelerating thereby decreasing the stay time in a given increment of length.

4.2. Variation of vaporization rate with axial distance

Vaporization rate is defined as percentage of mass vaporized divided by droplet velocity as follows

$$Vaporizatio\ rate\% = \frac{w/m_{d0}}{v_d} x100 \qquad 8$$

The curve showing the vaporization rate per length of chamber has two peak points and a minimum point (figure 3). The minimum point occurs when the gas velocity and droplet velocity are equal, producing a Reynolds number of zero. The vaporization rate is initially low because the vapor pressure (at the low initial temp.) is small, resulting in a low driving force for mass transfer. At the end of the chamber, the rate is also low, mainly because of the small surface area of the droplet.

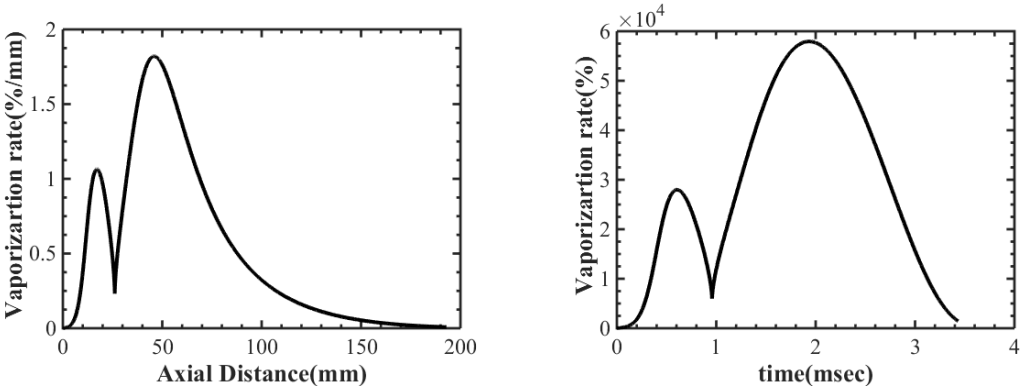

Vaporization rate vs. axial distance Vaporization rate vs. time

Figure 3. Vaporization rate variation for single heptane droplet

4.3. Histories of heptane spray in a cylindrical chamber

For this case, the input data are given in table 3

Table 3. Data for n-heptane spray case

Parameter	Value
Mass median radius [micron]	75
Initial droplet velocity [m/sec]	30
Chamber pressure [bar]	20
Standard deviation	2.3
Chamber gas temperature (K)	3100
Initial droplet temperature (R)	280
Chamber contraction ratio	3.15

The value of chosen standard deviation is the expected one for impinging jet [6], however other injectors have different value for standard deviation e.g. the geometric standard deviation is 3.5 for the parallel-sheet injector and 20 for the triplet injector [7]

From figure 4, it is clear that small droplets follow the gas-velocity curve, while the large droplets remain almost at the injection velocity. It is clear from figure 4 that the distance and time required to attain the wet-bulb temperature increase with droplet size.

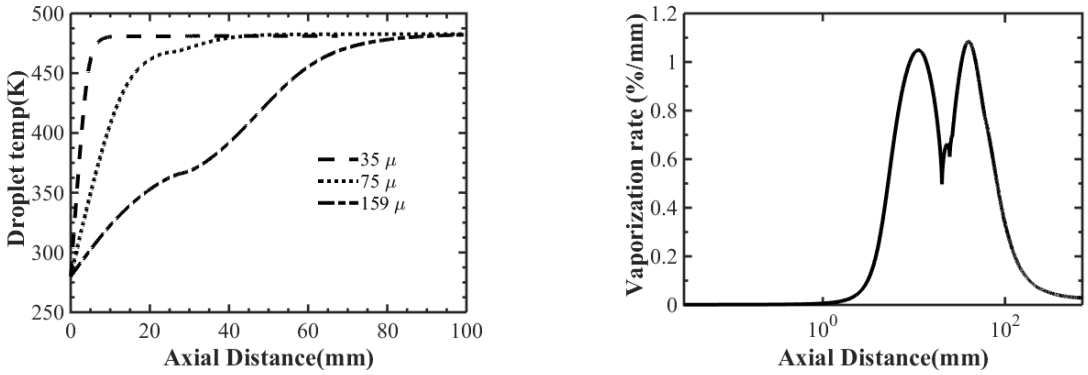

Variation of droplet temperature Variation of droplet radius

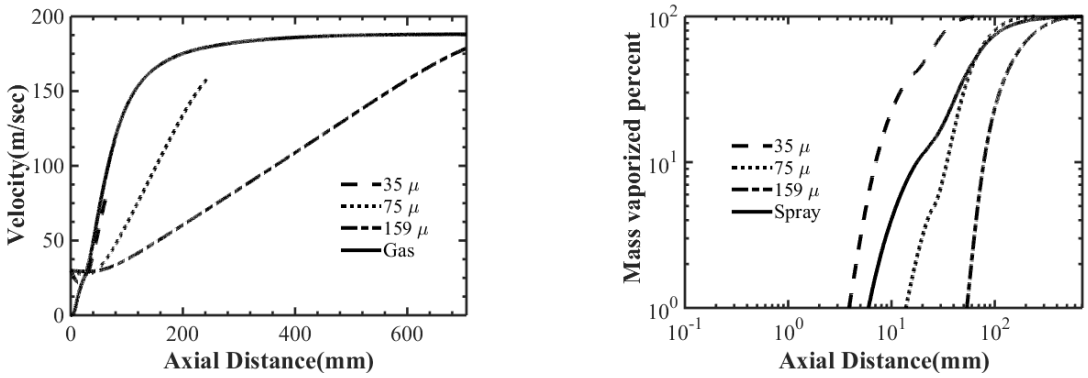

Variation of droplet and gas velocities Percentage mass vaporized

Figure 4. Variation of droplet temperatures, droplet velocities and percentage mass vaporized with axial distance for heptane spray

5. Case Studies

5.1. LOX/Kerosene engine (RD-0110)

The earliest liquid rocket engines used LOX and hydrocarbon, Goddard's first successful rocket flight in 1926 used LOX and gasoline, The Germen V-2 use LOX and aqueous ethanol solution. The heavy lift requirements of early ballistic missile in USA and USSR during cold war period necessitated the replacement of aqueous ethanol fuel with a kerosene petroleum distillate.

The RD-0110 is a rocket engine burning liquid oxygen and kerosene in a gas generator combustion cycle. It has four fixed nozzles and the output of the gas generator is directed to four secondary vernier nozzles to secure vector control of the stage. It has an extensive flight history with its initial versions having flown more than 58 years ago. It has been used in the Molniya-M Block-I and on most of the Soyuz Block-I

The term kerosene is used to describe a distillate fraction of petroleum boiling between (roughly) 200 and 300°C. Jet fuels are kerosene; naturally, jet fuels such as JP-4 were the initial kerosene used in rocket tests. In comparison to jet fuel, RP-1 has a much narrower allowable density range and lower limits on fuel components that were thought to cause deposits during regenerative cooling, such as sulfur, olefins, and aromatics [8]. Russian kerosene (RG-1, naphthyl, or T-1) is somewhat different from RP-1, notably with 3% higher density/specific gravity (0.832 vs. 0.806 at 22°C) and 21% less in sulfur contents, with lower temperature rise in cooling passage. In addition, it has better performance at lower mixture ratio [8]. Engine applications include the RD-180, RD-170, and NK-33.

For the fuel used in RD-0110, it has specific gravity of 0.845, heat of formation -6.9 kcal/mole; it can be represented as $CH_{1.9534}$

5.1.1. Engine data and description

The operating parameters of the engine used in comparison are presented in table 4. The fuel is fed at nozzle exit in order to cool the thrust chamber; the injection head has 91 bi-centrifugal injectors (figure 5, and table 5).

Table 4. RD-0110 engine data

Parameter	Value
Oxidizer Pump exit Pressure (bar)	98.1
Fuel pump exit pressure (bar)	132.4
Combustion pressure (bar)	68.16
Engine Mixture ratio	2.2
Thrust (kN) per chamber (4 chambers)	73.412
Specific impulse (sec)	336.429
Fuel mass flow rate (kg/sec)	6.6
Oxidizer mass flow (kg/sec)	15.7
Burning time (sec)	240
Chamber diameter (mm)	180
Cylindrical part length (mm)	~204

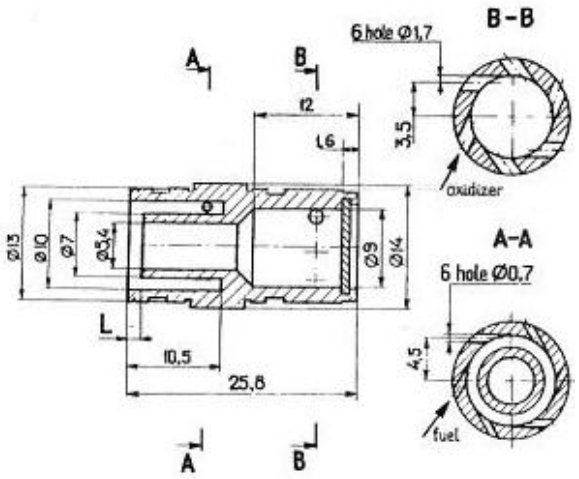

Figure 5. RD-0110 injector with dimensions

Table 5. RD-0110 injector data

Parameter	T-1	LOX
Mass flow rate(g/sec)	64.8	173
Spray angle(deg)	135	80
Swirl chamber diameter	8.5	9
Inlet port diameter	0.7	1.7
Number of inlet ports	6	6
Geometric parameter	24.5	2
Mass flow rate(g/sec)	64.8	173
Spray angle(deg)	135	80
Swirl chamber diameter	8.5	9

5.1.2. Transport properties of gaseous products

In order to evaluate the transport properties (viscosity, thermal conductivity) for the gaseous mixture, the gas mixture should be simplified to consider only the main species. There are two cases; case (a) using assumption of complete combustion (all carbon is converted to CO2, and all hydrogen is converted to H2O), and case (b) using equilibrium combustion products: In this analysis, case (b) is considered. Making use of the mixing laws [9]. the results of mixture properties are fitted as:

$$C_p = 29.34 + 0.009T \quad J/mole\ K$$
$$\mu = 5.41x10^{-6} + 3.3x10^{-8}\,T \quad Pa.\sec \qquad (9)$$
$$k = 0.002 + 0.0001T \quad W/m.K$$

5.1.3. Contraction ratio and final gas velocity

For the engine considered, the thrust chamber geometry gives contraction ratio of 4.538 from which final gas velocity or velocity at the end of cylindrical part can be calculated using isentropic flow relations to be 140 m/sec

5.1.4. Injection velocity

In order to find the injection velocity, the geometrical parameters of fuel and oxidizer injectors should be given in order to calculate discharge coefficient otherwise, measure discharge coefficients. Cold flow and hot flow measurements of discharge coefficient of this injector are performed in [10] (table 6).

Table 6. Discharge coefficient for injector in Kim et al. 2005

	Oxidizer(inner)	Fuel(outer)
Discharge coefficient (non-reacting)	0.37	0.045
Discharge coefficient (reacting)	0.35	0.042
Injection velocity (m/sec)	12.3	11.38

5.1.5. Fuel inlet Temperature

Assume the fuel entering the cooling passage at ambient temperature (300 K). The fuel injection can be assumed to be 350 K

5.1.6. Mean radius and Droplet size distribution

The SMD of the spray can be evaluated either by empirical formulae or by cold flow measurements. However, the suggested formula in literature for bi-centrifugal injector or even single swirl injector has geometry different from that of this injector. Using the data of cold flow measurements [10] for which SMD was reported to be about 200 μm using water instead of propellant. Using correction formula for change in physical properties $D_{30}\alpha\left(\frac{\mu_L\sigma}{\rho_L}\right)^{0.25}$ [11] to correct the SMD to the used fuel (table 7), this gives SMD of 198 μm.

Table 7. Physical properties used to correct SMD

	Density	Viscosity	Surface tension	SMD	$\overline{D}$	MMD
T-1(@ 323 K)	815	$1.93x10^{-3}$	$30x10^{-3}$	198	352	294

For this type of injector, Rosin-Rammler distribution is used, the distribution parameter may be assumed to vary from 2 to 5, take it equals 2.

5.1.7. Results and Discussion

Comparison of the length required for vaporizing 95% of fuel with the measured geometry of the thrust chamber is shown in table 8.

Table 8. Results for RD-0110 engine

		$L_{95\%}$
Case(a)	Uniform (D=198)	62.6
Case(b)	Spray (q=2, SMD = 198 μm)	147.2

From previous, it is found that calculations for spray is in good agreement with the actual motor (error=25 %). To have better agreement, breakup length (pre-vaporization length) should be added. Breakup length can be estimated to be between 20-30 mm. this give total atomization and vaporization length to be 170 mm giving error 15 %; this is expected as the propellant combination LOX/T-1 satisfies the limitation of model. And the difference in length may be due to some deviation from model assumptions of perfect mixing and infinite chemical reaction rates.

5.2. RFNA/Tonka250 engine

Earth-storable fuels and oxidizers were often used in early rockets, and their development accelerated during World War II. Drawing on German WWII Wasserfall missile, Nitric acid became the early storable oxidizer of choice for missile and upper stages of the 1950 and 1960s (e.g. first stage engine VEXIN of the French launch vehicle DIAMANT which uses RFNA/turpentine), to overcome various problems with its use, it was necessary to combine the nitric acid with NTO and passivation compounds. Various hydrocarbons were used as storable fuels (gasoline, jet fuel, etc.), the propellant combination WFNA/JP-4 and later IRFNA/JP-4 were first storable combination used in USA, which have the advantage of have high calorific value, remains liquid within wide temperature limits. However, the absence of reliable hypergolic ignition and unstable combustion cause abandon this combination to hypergolic combinations since a short ignition delay would minimize this accumulation and permit rapid, full flow start

5.2.1. Oxidizer composition and physical data

Of all the widely used oxidizer, nitric acid has the greatest specific gravity (1.4:1.5). In addition, nitric acid has boiling and freezing temperature (+86˚C and -42˚C) suitable for application in liquid rocket motor. In order to improve the properties of nitric acid as an oxidizer, it is mixed with various additives, this produces variety of nitric acid formulation; Red Fumed Nitric Acid (RFNA) based on anhydrous nitric acid with addition of 13 % NTO and 3 % H2O.and Inhibited Red Fumed Nitric Acid (IRFNA), based on RFNA with addition of 0.6 % HF which act as a corrosion inhibitor.

In this study, RFNA is considered as 78% Nitric Acid, 20% Nitrogen tetroxide and 2% H2O, this result in specific gravity of 1.478, freezing point -60° C and boiling temperature of 49.5 and heat of formation of -59.92 kcal/mole. With summary formula of

$$H_{1.460}N_{1.673}O_{4.695}$$

5.2.2. Fuel composition and physical properties

Throughout the late 1940s and early 1950s, a large number of storable fuels were tried with nitric acid. Several self-igniting fuels were found; for example Aniline, furfuryl alcohol, xylidine, triethylamine and hydrazines.

Triethylamine-which primarily used as an additive to rocket fuels to reduce viscosity-may have synergetic effect to reduce ignition delay take place, that the ignition delay of the mixture is less than the ignition lag of either pure substance. This give rise to the mixture of triethylamine .and xylidine which first developed in Germany and named was Tonka 250[12].

In this study fuel is considered as mixture of 50% Xylidine, 48.5% tri-ethylamine and 1.5% di-ethylamine, with specific gravity 0f 0.845, Heat of formation -12.04 kcal/mole, and summary formula

$$C_{6.276}H_{11.971}N_{0.908}$$

5.2.3. Engine data and Description

The engine used in comparison has the operating parameters presented in table 9.

Table 9 Engine using RFNA\Tonka250 data

Oxidizer Pump delivery(kg/sec)	10
Fuel pump delivery(kg/sec)	3
Combustion pressure(bar)	52
Mixture ratio	3.35±0.2
Thrust (kN)	31±2
Specific impulse(sec)	231
Cylindrical part length(mm)	**265**

The oxidizer is fed at nozzle exit in order to cool the thrust chamber; the injection head have 79 bi-centrifugal injector (figure 4) + 36 circumferential fuel holes. The circumferential fuel holes are used to provide film cooling in addition to regenerative cooling done by oxidizer.

The construction of the bi-centrifugal injector is shown in figure 4

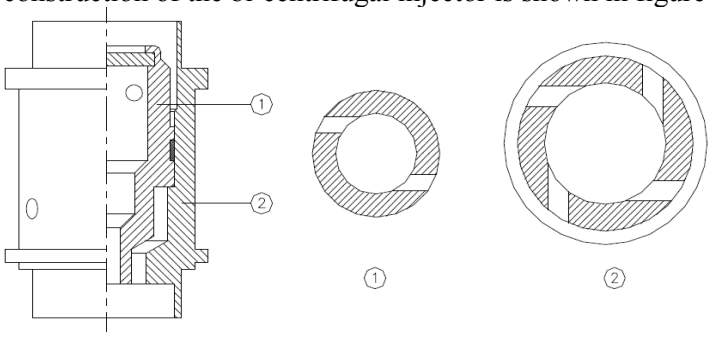

Figure 6. The bi-centrifugal injector used in [13]

Ramezani1 and Ghafourian (2005) studied a similar injector to case study, hence, Discharge coefficient a will be taken from their data. The dimensions of this injector are indicated in table 10.

Table 10 Dimensions for the injector used in [13]

	d_0	D_p	D_s
Inner injector	2	1.2	6
Outer injector	5.8	1.5	9

5.2.4. Transport properties of gaseous products

As in the previous case. The results of mixture properties are fitted as:-

$$C_p = 30.0668 + 0.0102T \quad J/mole\ K$$

$$\mu = 44.6045x10^{-6} + 3.471x10^{-8}T \quad Pa.\sec \qquad 10$$

$$k = -0.0044 + 0.0001T \quad W/m.K$$

5.2.5. Contraction ratio and final gas velocity

For the engine considered, measurements of the thrust chamber geometry gives contraction ratio of 6, from which final gas velocity or velocity at the end of cylindrical part can be calculated using isentropic flow relations to give final gas velocity 102 m/sec

5.2.6. Injection velocity

As mentioned above, there are experimental data for an injector which is largely similar to this engine's injector, from these data the discharge coefficients for fuel 0.21 and oxidizer 0.17.this results in injection velocity for oxidizer 12.668 m/sec and 37.846 m/sec for fuel

5.2.7. Inlet Temperature

Assume the oxidizer entering the cooling passage at ambient temperature (300 K). The rise in oxidizer temperature can be calculated by the algorithm mentioned in Barrère (1960) or Ludvik and Konecny (2002). The injection temperature of oxidizer found to be around 345 K. while injection temperature of fuel can be taken as 300 K.

5.2.8. Mean radii and Droplet size distribution

Most of researches were confined to single swirl injector, however, Han et al [14] quoted and modified Lefebvre's equation [15] and introduced the equation as

$$SMD = 2.25\,\sigma^{0.25}\,\mu_L^{0.25}\,\dot{m}_L^{\,0.25}\,\Delta P_L^{-0.5}\,\rho_g^{-0.25}\,f_c \qquad 11$$

where f_c is the combined geometric function which reflects the influence of geometric parameters on SMD, and can be calculated from

$$f_c = \frac{(\dot{m}U)_F\, f_F + (\dot{m}U)_O\, f_O}{(\dot{m}U)_F + (\dot{m}U)_O} \qquad 12$$

where f_F and f_O are the geometric function for inner and outer swirl injector alone, and can be calculated from as in equation A.3

$$f = \left(\frac{l_0}{d_0}\right)^{0.03}\left(\frac{L_s}{D_s}\right)^{0.07}\left(\frac{A_p}{D_s\, d_0}\right)^{-0.13}\left(\frac{D_s}{d_0}\right)^{0.21} \qquad 13$$

If Eqn.10 is used which is mainly suggested for bi-centrifugal injector, it is clear that the larger SMD is for RFNA @ 300 K. which may be taken as the value used in calculation. In addition, there is some experimental measurements for SMD for an injector that is greatly similar to this one [16]. The SMD in that experiment varies from nearly 120 μm near hollow cone region to reach maximum value of 140 μm at middle of spray region, which is corrected for different fuel/oxidizer properties. Results are indicated in tables 11, 12 (taking experimental SMD=130)

Table 11. SMD of RFNA/Tonka250 from empirical equation (10)

	SMD (μm)			SMD (μm)	
RFNA @ 300 K	without f	74.5	Xylidine	without f	40.7
	with f	98.97		with f	63.8
RFNA @ 345 K	without f	69.5	Triethylamine	without f	25
	with f	92		with f	39

Table 12. SMD for RFNA/Tonka250 using correcting formula to data in [16]

Case	Density	Viscosity	Surface tension	SMD(μm)
RFNA @ 300 K	1505	$7.89x10^{-4}$	0.039	94
RFNA @ 345	1427	$4.93x10^{-4}$	0.0297	79
Triethylamine	722.8	$3.345x10^{-4}$	0.0201	77
Xylidine	948	0.0013	0.0357	117

6. Results and Discussion

From above, there are two cases that should be considered (table 13) to compare the length required to vaporize 95 % of fuel/oxidizer with the measured geometry of the thrust chamber

Table 13. Cases considered with their results

		Propellant	Td(K)	V_{in}	$L_{95\%}$(mm)
Case (a)	Uniform (D=98 μm)	Oxidizer	300	12.6	31.9
	Spray (q=2, SMD=98 μm)				85
Case (b)	Uniform (D=117 μm)	Fuel	300	37.8	47
	Spray (q=2, SMD=117 μm)				150.6

This shows that the model prediction is far from real dimension (min error 43 %); this is expected as experience showed that in case of reaction involving nitric acid and hydrocarbon, the slow decomposition of gaseous NO to N2 is the rate limiting step which requires additional length to derive reaction to completion.[17], [18].

7. Conclusion and Future Work

In this work, the vaporization-controlled model was discussed; it has been shown that the model agrees well for LOX/kerosene combination but give bad estimation in case of RFNA/Tonka250 case. This can give idea about limitation of this model. These limitations can be summarized in the following:

- All the heat for vaporization comes from the hot gases,
- No breakup or interactions between droplets occur, and
- Instantaneous mixing and reaction are obtained.

The first limitation is violated for *hypergolic propellants* or *mono-propellants* that have liquid-phase reaction. With these conditions the vaporization rate would be increased, depending on the rate of the liquid-phase reaction. *The second limitation* is violated for droplets with a large velocity difference between the gas and droplets. With a large velocity difference, a critical Weber number (We=10) would be exceeded and the droplets would shatter. Shattering would increase the vaporization rate and produce higher performances than predicted by the vaporization model. *The third limitation* is violated either when (i) Propellants with very low reaction rates which are most likely to happen at very low chamber pressures or for propellant combination involving nitric acid and hydrocarbon group or (ii) With an injector that does not have a uniform distribution of propellants; there would be variations in the mixture ratio across the chamber hence mixing efficiency is not 100 %.

7.1. Future Work

The limitation of Priem's basic model, can be relaxed e,g; *two flame- front* models may be added for cases like exothermic droplet burning . *Incomplete spray mixing* and the resultant *mixture-ratio-striated gas flow* are quite important contributors to performance losses. In addition, mixing and vaporization losses maybe coupled, i.e., lower evaporation efficiencies maybe experienced in striated flows than in uniform flow, or vice versa.

In addition, this model was the responsible for the concept of "*the finer the spray, the better performance*" which was found to be incorrect in cases when the performance is controlled by the vaporization of both fuel and oxidizer as in NTO/MMH systems. It was found that optimum performance at certain droplet size increasing or decreasing droplet size leads to poorer performance.[19]. Chiu et al [20] introduced new concept of optimizing combustors, the concept is "minimum length of combustor is attributed to rapid axial development of combustion rate not to rapid vaporization" as rapid vaporization of fuel/oxidizer cause formation of fuel/oxidizer rich clouds which hinder further evaporation and reaction. In the next chapter, comprehensive combustion model is introduced with all sub-models; turbulence model, combustion model, two-phase coupling.

8. References

[1] Barrère M. et al. (1960) "Rocket propulsion" Elsevier Publishing Company, New York
[2] Riebling R. W. (1967)"Criteria for optimum propellant mixing in impinging-jet injection elements" Journal of spacecraft and rockets Vol.(4),pp 816-818
[3] Bittker D.A (1958) "An analytical Study of Turbulent and molecular mixing in rocket combustion" NASA TN-4321.
[4] Ferrenberg A. J. and Varma M. S. (1985) "Atomization data for spray combustion modeling" AIAA 1985-1316.
[5] Priem R. J. and Heidmann M.F. (1960) "Propellant vaporization as a design criterion for rocket engine combustion chamber" NASA TR R-67.
[6] Ingebo R. D (1958) "Drop Size Distributions for impinging-jet break-up in airstreams simulating the velocity conditions in rocket combustor" NASA TN-4222
[7] Priem R. J. (1958) "Propellant vaporization as a criterion for rocket engine design; Calculation of chamber length to vaporize various propellant" NACA TN-3883
[8] Edwards Tim (2003) "Liquid Fuels and Propellants for Aerospace Propulsion:1903–2003" Journal of propulsion and power Vol.(23),pp1089-1107
[9] Kee R J. et al. (1986)"A FORTRAN computer code package for the evaluation of gas-phase multi-component transport properties" SAND86-8246 (1986)
[10] Kim S.H. et al. (2005) "Effect of LOX post recess on the combustion characteristics of bi swirl coaxial injector" AIAA 2005-4445
[11] Ingebo R.D. and Foster H. (1957) "Drop size distribution for crosscurrent breakup of liquid jet in air stream" NASA TN 4087
[12] Morrell G. (1957) "Summary of NACA research of ignition lag of self-igniting fuel-nitric acid propellants" NASA RM E57G19
[13] Ramezani A.R. and Ghafourian (2005)"Spray Angle Variation of Liquid-Liquid Swirl Coaxial Injectors" AIAA 2005-3747
[14] Han P.G. et al. (2003)'The Spray Characteristics of Swirl Coaxial Injectors" AIAA 2003-0490
[15] Lefebvre A.H.(1989)"Atomization and sprays" , Taylor and Francis Publishing group
[16] Soltani M.R. et al. (2005) "Spray Characteristics of a liquid-liquid coaxial swirl atomizer at different mass flow rates" Aerospace science and Technology Vol. (9) pp 592-604
[17] Feiler C.E and Baker L. Jr. (1956) "A study of fuel-acid reactivity" NASA RM E56A19
[18] Miller R.O. (1955) "Flame propagation limits of propane and n-Pentane in oxides of Nitrogen" NASA TN 3520
[19] Jiang T.L. et al. (1992)"Numerical simulation of variable thrust engine combustion chamber" AIAA 1992-3769
[20] Chiu H.H. and Jiang T.L.(1987)"A new design approach of compact high performance liquid rocket engine combustors" AIAA 1987-2033.